Journal of Ceramic Processing Research. Vol. 25, No. 6, pp. 1042~1051 (2024)
(Received 30 August 2024, Received in revised form 24 September 2024, Accepted 5 November 2024)
https://doi.org/10.36410/jcpr.2024.25.6.1042

J O U R N A L O F
Ceramic Processing Research

Enhanced photocatalytic activity of electrospun TiO_2/Ag@SiO_2 inorganic composite nanofibers toward colored organic dye

Hyung Jun Lim, Gyu Il Jung, Da Young Kang and Sang Man Koo*
Department of Chemical Engineering, Hanyang University, Seoul 04763, Korea

Inorganic composite nanofibers consisting of TiO_2, metallic Ag, and SiO_2 nanoparticles were prepared using electrospinning to enhance photocatalysis of a colored organic dye. Inorganic composite nanofibers have a high surface-area-to-mass ratio and are suitable for various applications in catalysis, sensors, and environmental remediation. In this study, TiO_2 and metallic Ag nanoparticles were homogeneously embedded in a phenylsilsesquioxane matrix by mixing molecular precursors such as titanium diisopropoxide bis(acetylacetonate) and Ag-neodecanoante with phenyltrimethylsilane-based organically modified silica particles dissolved in dimethylformamide. Electrospinning transformed these precursor mixtures to hybrid composite nanofibers. Subsequent application of heat at 1000 °C converted the hybrid composite nanofibers to inorganic composite nanofibers. Metallic Ag nanoparticles were used in the design of the composite photocatalyst to enhance its photocatalytic activity by exploiting the band gap overlap between metallic Ag and semiconducting TiO_2 particles. Inorganic composite nanofibers without having Ag nanoparticles were also prepared for comparison purposes using only Ti and Si precursors. Rhodamine B was selected to test the photocatalytic activities of both inorganic composite nanofibers, and ultraviolet (UV)-visible light spectroscopy was used to investigate the photocatalytic activities of the inorganic composite nanofibers. Under UV light, TiO_2/Ag@SiO_2 inorganic composite nanofibers were more efficient than TiO_2@SiO_2 inorganic composite nanofibers. X-ray diffraction, transmission electron microscopy–energy-dispersive spectroscopy, and X-ray photoelectron spectroscopy confirmed the uniform distribution of TiO_2 and Ag nanoparticles in the corresponding composite nanofibers.

Keywords: Inorganic composite nanofibers, Electrospinning, ORMOSIL particles, TiO_2/Ag nanoparticles, Photocatalyst.

Introduction

Contamination of the air and water is causing serious public concerns about human and ecosystem health [1]. Among the methods available to address such pollution, photocatalysis has received extensive attention because it is a low-impact technology that can be used at normal temperatures and pressures [2, 3].

Most photocatalytic processes use the particulate forms of catalysts because of the superior photocatalytic efficiency provided by the large surface-to-volume ratio related to size reduction [4, 5]. However, separating microscopic photocatalysts from a reaction medium after completion of the photocatalytic process can be difficult [6]. In addition, such small particles have a strong tendency to agglomerate into larger particles, resulting in a reduction in photocatalytic activity [7, 8]. To optimize photocatalytic performance in commercial applications, nanosized catalyst particles in and/or on substrates with a large surface area, such as one-dimensional material, are often dispersed [9]. Electrospinning is a versatile and cost-efficient method for the large-scale production of one-dimensional nanofibers with a high surface-to-volume ratio [10, 11]. Electrospun one-dimensional nanofibers can be applied to catalysts, sensors, filters, and batteries [12-15]. Early studies focused on spinning organic polymer nanofibers, but research on electrospinning technologies has expanded to include inorganic and composite nanofibers, and materials are no longer limited to polymers.

Titanium dioxide (TiO_2) is one of the most effective metal-oxide semiconductors among those that have been extensively investigated and used in catalysts, solar cells, sensors, and other optical and electronic devices due to its low cost and nontoxic and environmentally friendly characteristics [16-18]. It is also associated with outstanding electronic and optical properties and stability. TiO_2 exhibits three crystalline phases: anatase, rutile, and brookite. The photocatalytic activity of TiO_2 is strongly affected by its physical characteristics, including crystallization, grain size, morphology, surface area, surface state, and porosity [19-21]. TiO_2 fibers were first fabricated by electrospinning in 2003 [22]. He et al. studied electrospun TiO_2 fibers as photocatalysts that can degrade dye pollutants [23]. Based on these studies, TiO_2-based fibers with a large aspect ratio were fabricated to mitigate the disadvantages of nanosized particulate TiO_2 catalysts. However, TiO_2 presents some drawbacks,

*Corresponding author:
Tel : +82-10-3617-1910
E-mail: sangman@hanyang.ac.kr

such as a relatively wide band gap of 3.2 eV and a high recombination rate of photo-generated electron-hole pairs, hindering its application as a photocatalyst [24, 25]. These disadvantages can be addressed with the addition of other metal-oxide semiconductors or metallic particles that can facilitate charge transfers by decreasing the band gap of TiO_2. Recently, tests of noble metals with low resistance, such as silver (Ag), gold (Au), and platinum (Pt), indicate that they can effectively accelerate the decomposition of organic dye molecules by prohibiting electron-hole recombination through the separation of photo-generated electron-hole pairs and the promotion of interfacial charge transfers [26-31].

In this study, inorganic composite nanofibers consisting of TiO_2, metallic Ag, and SiO_2 nanoparticles fabricated by electrospinning were used to enhance the photocatalysis of colored organic dyes. Metallic Ag was used as an electron mediator due to its electronic conductivity, stability, and strong surface plasmon resonance effect [32-36]. A precursor solution for composite hybrid nanofibers was prepared by mixing phenyltrimethoxysilane (PTMS)-based organically modified silica (ORMOSIL) particles with titanium diisopropoxide bis(acetylacetonate) and Ag-neodecanoate (Ag-ND) in N,N-dimethylformamide anhydrous (DMF). The elementary composition and morphology of composite nanofibers (TiO_2@SiO_2 and TiO_2/Ag@SiO_2) were investigated using field emission scanning electron microscopy (FE-SEM), transmission electron microscopy (TEM), X-ray diffraction (XRD), and X-ray photoelectron spectroscopy (XPS). The ability of inorganic composite nanofibers to photocatalyze rhodamine B under ultraviolet (UV) light was then examined. The inorganic composite nanofibers can be easily recycled by centrifuging, washing, and drying without any noticeable reduction in photocatalytic activity. Our observations suggest that the inorganic composite nanofibers developed in this study can be used in a broad range of applications in environmental remediation.

Experimental

Materials

Phenyltrimethoxysilane (PTMS, 97%, Alfa-Aesar) and ammonium hydroxide (NH_4OH, 25-28 wt.% NH_3, Daejung Chemicals and Metals) were used to prepare PTMS-based ORMOSIL particles. Silver nitrate ($AgNO_3$, 99.8%, Junsei), neodecanoic acid (NDA, 99.8%, STREM), and sodium hydroxide (NaOH, 98%, Daejung Chemicals and Metals) were used to synthesize silver neodecanoate (Ag-$O_2C_{10}H_{19}$, Ag-ND). Titanium (IV) diisopropoxide bis(acetylacetonate) in 75 wt.% isopropanol ($Ti(acac)_2(O^iPr)_2$, STREM) was used as a precursor to prepare TiO_2 nanoparticles. DMF (99.8%, Sigma-Aldrich) was used as an organic solvent to prepare a precursor solution. Methanol (99.5%, Daejung Chemicals and Metals) and deionized (DI) water were used as washing solvents. All chemicals were used without further purification.

Preparation of PTMS-based ORMOSIL particles

ORMOSIL particles based on PTMS particles were prepared as reported previously [37]. Initially, 100 mL of DI water and 0.1 mL of NH_4OH (2.9 mmol) were added to a three-necked flask. The temperature of the reaction solution was adjusted to 70 °C, and the solution was stirred at 350 rpm. After 10 min of stirring, 14.36 mL of PTMS (0.0775 mol) was added to the solution using a syringe, after which the reaction mixture was stirred for 3 h. PTMS-based ORMOSIL particles were formed by hydrolysis and condensation reactions of phenylsilane monomers, resulting in a white suspension. After 3 h, the resulting solution was filtered through a membrane, and PTMS-based powders were washed several times with DI water and methanol. After drying in a vacuum oven at 110 °C for 2 h, 9.98 g of PTMS-based ORMOSIL particles (a yield of 99.8%) were obtained.

Preparation of silver neodecanoate (Ag-ND)

In a typical synthesis procedure, 0.0179 mol of NaOH was dissolved in 50 mL of DI water, and the same molar amount of NDA was added. The reaction temperature was adjusted to 50 °C and the solution was stirred for 1 h. Next, 50 mL of an aqueous solution of $AgNO_3$ (0.0179 mol) was added to the solution and the mixture was stirred for an additional 1 h, resulting in precipitation of a white powder. The resulting suspension was filtered through a membrane, washed several times with DI water, and finally washed with MeOH. The product was dried in a vacuum oven at 30 °C for 12 h, producing 4.44 g of silver Ag-ND powder at a yield of 88.8%.

Preparation of precursor solutions for electrospinning

A precursor solution of TiO_2@SiO_2 composite hybrid nanofibers was prepared by mixing $Ti(acac)_2(O^iPr)_2$ and PTMS-based ORMOSIL particles. 3.0 g of PTMS-based ORMOSIL particles was dissolved in 1.05 g of anhydrous DMF and $Ti(acac)_2(O^iPr)_2$ was then added to the dissolved solution at a molar ratio of 2:1. To manufacture TiO_2/Ag@SiO_2 composite hybrid nanofibers, additional Ag-ND was added to the precursor solution at a molar ratio of 1:1 for Ti and Ag. The resulting precursor solution was stirred at 240 rpm for 1 h at 100 °C, adjusting the viscosity to about 140 poise, suitable for electrospinning.

Fabrication of composite hybrid nanofibers using electrospinning and thermal conversion to inorganic composite nanofibers

Lab-type electrospinning equipment (NNC-ESP200) from Nano NC was used to produce composite hybrid nanofibers. Composite hybrid nanofibers were fabricated by electrospinning with the corresponding precursor.

The prepared precursor solution was loaded into a 3 mL plastic syringe equipped with a 15-gauge stainless-steel spinneret. The metallic needle was connected to a high-voltage power supply, and the precursor solution was supplied through the needle at a constant rate of 1 mL/h while a voltage of 8-10 kV was applied to inject electric charges. The resulting as-spun composite hybrid nanofibers were collected on a grounded aluminum-foil substrate at a tip-to-collector distance of 15 cm. Electrospinning was carried out at room temperature. After electrospinning, as-spun composite hybrid nanofibers were transferred to a vacuum oven at 80 °C for drying and then moved to a muffle furnace for annealing at 1000 °C in air at a heating rate of 10 °C/min to produce inorganic composite nanofibers. Inorganic TiO_2@SiO_2 composite nanofibers and TiO_2/Ag@SiO_2 composite nanofibers were obtained and used to investigate photocatalytic activity toward an organic dye molecule (rhodamine B) under UV light.

Surface etching of inorganic composite nanofibers

To further increase photocatalytic efficiency, the surface of inorganic composite nanofibers was partially etched by an aqueous hydrofluoric acid (HF) solution, increasing the surface area of the inorganic composite nanofibers and exposing photocatalytically active TiO_2 and metallic Ag nanoparticles. A 1 g sample of each inorganic composite nanofibers was immersed in 0.5 M aqueous HF for 10 min, washed three times with DI water, and dried at 60 °C for 3 h.

Evaluation of photocatalytic activity for degradation of rhodamine B

A 0.01 g sample of inorganic composite nanofibers (TiO_2@SiO_2 and TiO_2/Ag@SiO_2) was added to 30 mL (1×10^{-5} M) of an aqueous solution of rhodamine B. The mixture was wrapped with aluminum foil to prevent exposure to light and then stirred in the dark for approximately 30 min to obtain an absorption-desorption equilibrium condition prior to irradiation. A UV light source (300-420 nm) with a maximum intensity of 7.6 mW/cm^2 at 365 nm was used to irradiate the reaction mixture at a distance of 15 cm. The rhodamine B remaining after photodegradation was detected by UV-visible light spectroscopy at 554 nm. The change in the concentration of rhodamine B was monitored by extracting 3 mL of the solution with a syringe from the reaction mixture at fixed time intervals (30, 60, 90, 120, and 180 min after commencement of irradiation) and transferring it to vials for absorbance measurement with a UV-visible light spectrophotometer. Photocatalytic activity for TiO_2@SiO_2 and TiO_2/Ag@SiO_2 inorganic composite nanofibers after surface etching were also evaluated. To investigate the recyclability of inorganic composite nanofibers, the photocatalysts underwent three continuous cycles of photocatalysis of rhodamine B under identical experimental conditions.

Characterizations

The morphologies of the electrospun composite hybrid nanofibers were observed by FE-SEM (JEOL JSM-6340F) and optical microscopy (Olympus BX51). FE-TEM (JEOL JEM-3010) was used to investigate the morphologies and the distribution of chemical constituents (TiO_2 and metallic Ag) of inorganic composite nanofibers before and after surface etching. Surface analyses of the inorganic composite nanofibers were also conducted using EDS in TEM and XPS (PHI Quantera II) with Al-Kα monochromatic radiation of 1486.6 eV. To analyze the development of the crystalline phases of TiO_2 nanoparticles and metallic Ag nanoparticles in inorganic composite nanofibers along with the temperature change, XRD (Rigaku D/RAD-C) patterns were obtained using a diffractometer with Cu-Kα radiation (λ = 1.5418 Å) at 40 kV and 100 mA. To evaluate the photocatalytic ability of inorganic composite nanofibers, changes in dye concentration during the photodegradation of rhodamine B were measured using a UV-visible light absorption spectrometer (Scinco S-4100).

Results and Discussion

Scheme 1 illustrates the fabrication process of inorganic composite nanofibers used in the photocatalytic degradation of colored organic dye. In the first stage of preparation, precursor solutions for electrospinning were prepared by homogeneous mixing of corresponding chemical species in each composite nanofiber. For TiO_2@SiO_2 composite hybrid nanofibers, $Ti(acac)_2(O^iPr)_2$ was used as a Ti source and PTMS-based ORMOSIL particles were used to supply silicon at molar ratios of 2:1. Compared to silica particles, PTMS-based ORMOSIL particles are softer and even soluble in some organic solvents, which makes them suitable for reprocessing, such as filming and electrospinning. This versatility in structural modification might come from the fact that a relatively lower degree of condensation occurs during the sol-gel process due to the steric hindrance from bulky phenyl groups in PTMS [38]. ^{29}Si-NMR result in a previous study indicated that the PTMS-based ORMOSIL particles are consisted of the structural network with 27% of partially condensed T^2 units and 73% of fully condensed T^3 units [39]. This unique structural property of PTMS-based ORMOSIL particles can provide additional processability while maintaining morphological stability as a particulate form. In the TiO_2/Ag@SiO_2 composite hybrid nanofibers, Ag-ND was also used as an Ag source. DMF was used as a solvent for mixing and to control viscosity. When the molar ratio of Ti to Si was less than 4:1, no crystalline TiO_2 was observed after heat treatment, probably due to the low levels of TiO_2 in the composite nanofibers. When a molar ratio of 1.5:1 was used, the resulting as-spun composite hybrid nanofibers were partially melted, exhibiting a loss of fiber shape. An optimal molar ratio of Ti to Si was set at 2:1 to achieve the highest TiO_2

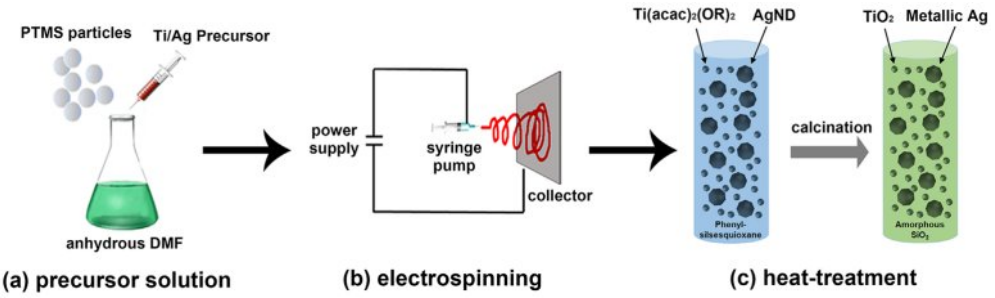

Scheme 1. The fabrication process of inorganic composite nanofibers by electrospinning.

content in composite hybrid nanofibers and maintain their structural integrity through the electrospinning process.

Metallic Ag in the TiO_2/Ag@SiO_2 composite nanofibers was used as an electron mediator due to its electronic conductivity, stability, and strong surface plasmon resonance effect. Particles of noble metals can enhance charge transfer by decreasing the band gap of TiO_2, accelerating the decomposition rate of organic dyes by prohibiting electron-hole recombination [40-42]. In the second step, composite hybrid nanofibers were fabricated by electrostatic spinning of precursor solutions. The precursor solution was supplied through a needle at a constant rate of 1 mL/h, while a voltage of 8-10 kV was applied to inject electric charges. The resulting as-spun composite hybrid nanofibers were collected on a grounded aluminum-foil substrate at a 15 cm distance between the syringe tip and the collector. Electrospinning was carried out at room temperature. Afterward, as-spun composite hybrid nanofibers were dried in a vacuum oven at 80 °C for 1 h, followed by heating to 1000 °C in the air at 10 °C/min.

The morphology of as-spun composite hybrid nanofibers was investigated by SEM and optical microscopy, as shown in Fig. 1. These composite nanofibers appear as a one-dimensional structure with a random orientation. Fig. 1(a) shows that TiO_2@SiO_2 composite hybrid nanofibers present with a smooth surface, with diameters ranging from 85 to 320 nm and lengths of a few micrometers. Fig. 1(b) exhibits the randomly aligned linear fibers with homogenous surfaces of the TiO_2/Ag@SiO_2 composite hybrid nanofibers with diameters varying from 76 to 132 nm.

Detailed morphologies and internal microstructures of inorganic composite nanofibers, before and after surface etching, were scrutinized by FE-TEM (Fig. 2). TEM confirmed that TiO_2 and Ag nanoparticles were distributed homogeneously in all inorganic composite nanofibers and were in intimate contact. Under a UV light source, TiO_2 undergoes an electron transition and generates electron-hole pairs. However, this electronic transition is not stable, and photo-generated electron-hole pairs may be annihilated by a recombination process. These shorter-lived photo-generated electrons and holes often decrease the photocatalytic efficiency by reducing their availability for participation in photocatalytic reactions. It has been reported that noble metals (Ag, Au, and Pt) with an unfilled d-electron structure have a strong tendency to transfer and accommodate photo-generated electrons from the conduction band of TiO_2, while photo-generated holes remain on the valence band of the TiO_2. This results in the formation of Schottky barriers at the Ag-TiO_2 contact region and gives rise to charge separation [43]. In this study, metallic Ag particles dispersed with TiO_2 nanoparticles act as an electron trapping center by immobilizing the photo-generated electrons and preventing the electron-hole pairs recombination.

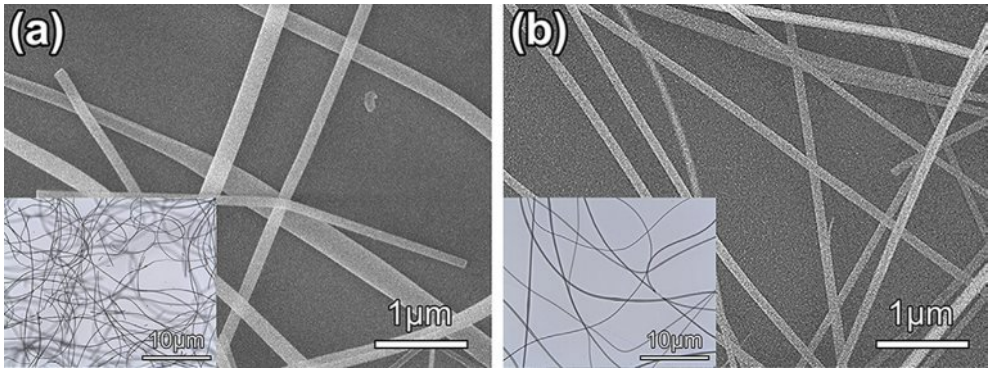

Fig. 1. FE-SEM and OM (inset) images of as-spun composite hybrid nanofibers: (a) TiO_2@SiO_2 composite hybrid nanofibers and (b) TiO_2/Ag@SiO_2 composite hybrid nanofibers.

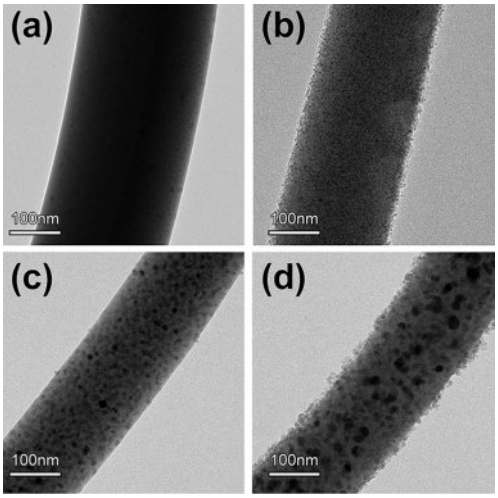

Fig. 2. TEM images of inorganic composite nanofibers before (left) and after (right) surface etching with an aqueous HF solution: (a) TiO_2@SiO_2 inorganic composite nanofibers and (b) TiO_2/Ag@SiO_2 inorganic composite nanofibers.

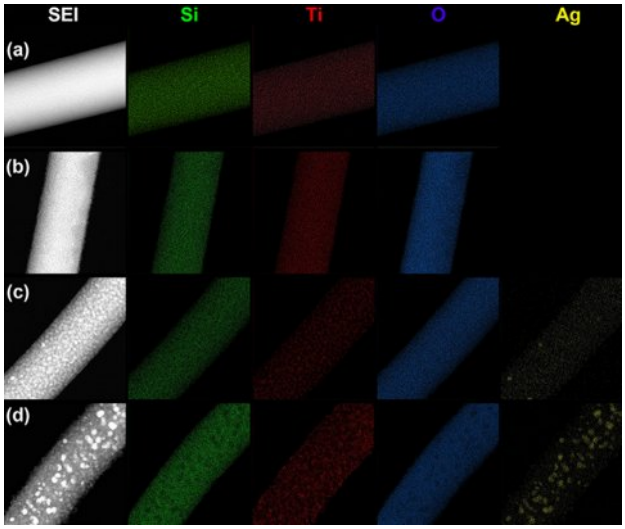

Fig. 3. TEM-EDS mapping of Si, Ti, O, and Ag elements on the surface of inorganic composite nanofibers: TiO_2@SiO_2 inorganic composite nanofibers before (a) and after (b) surface etching and TiO_2/Ag@SiO_2 inorganic composite nanofibers before (c) and (d) after surface etching.

Surface etching of inorganic composite nanofibers using an aqueous HF solution can increase the photocatalytic ability further by exposing the photocatalytically active TiO_2 and metallic Ag species. The TEM image in Fig. 2 shows that the nanoparticles are exposed on the surface of inorganic composite nanofibers after surface etching with HF. All inorganic composite nanofibers retained their original shape, even after surface etching. As shown in Fig. 2(a) and (b), TEM images of TiO_2@SiO_2 inorganic composite nanofibers show evenly distributed uniform TiO_2 and SiO_2 nanoparticles inside inorganic composite nanofibers. After surface etching with an aqueous solution of HF for 10 min, the surface of inorganic composite nanofibers became rough with exposure of fine TiO_2 nanoparticles on their surface. Fig. 2(c) and (d) show TEM images of TiO_2/Ag@SiO_2 inorganic composite nanofibers consisting of evenly distributed metallic Ag and TiO_2 nanoparticles with an average size of 14.2 (±4.5) nm and 4.5 (±0.6) nm, respectively.

The surface chemical compositions of the TiO_2/Ag@SiO_2 inorganic composite nanofibers before and after surface etching were further determined by TEM-EDS measurements (Fig. 3). The EDS mapping images in Fig. 3 confirm that Si, Ti, O, and Ag elements are uniformly distributed along the fiber body. After surface etching, the distribution of Ti and Ag on the surface appeared to be thicker and brighter than before etching due to the removal of a SiO_2 layer on the surface. From the result of TEM and EDS analyses, it can be concluded that the surface area and the amount of photo-catalytically active species such as TiO_2 and metallic Ag nanoparticles are increased by surface etching with HF. Especially for surface etched TiO_2/Ag@SiO_2 inorganic composite nanofibers, the roughest exteriors and well-defined nanoparticles of TiO_2 and metallic Ag are observed on the surface of inorganic composite nanofiber, which results in a pronounced improvement in photocatalytic activity.

Fig. 4 depicts XRD patterns of TiO_2@SiO_2 and TiO_2/Ag@SiO_2 composite nanofibers after heat treatment at three temperatures in the air. Neither composite nanofiber, when dried at 80 °C, produced a discernible diffraction peak, indicating that Si, Ti, and Ag elements existed as molecular species or amorphous states at this temperature. After heat treatment at 800 °C, a small peak at a 2θ value of 25° from the crystalline anatase phase of TiO_2 was observed for TiO_2@SiO_2 composite nanofibers, while two peaks at 2θ values of 25° and 48° from the crystalline anatase phase of TiO_2 as well as several moderate peaks at 2θ = 38°, 44°, 64°, and 77° from the face-center cubic phase of metallic Ag were observed for TiO_2/Ag@SiO_2 composite nanofibers [41, 44]. This implies that the conversion of TiO_2 to an inorganic phase began at this temperature, although the transformation of Ag precursor to a metallic phase occurred at a temperature lower than 800 °C. After heat treatment at 1000 °C, the intensities of diffraction peaks from the anatase phase of TiO_2 and metallic Ag increased further, with well-grown crystalline peaks evident for both inorganic composite nanofibers: 25.4°(101), 36.4°(004), 48.2°(200), 54.2°(105), 55.4°(211), and 62.7°(204) for the anatase phase of TiO_2 (JCPDS No. 21-1272) and 38.3°(111), 44.4°(200), 64.4°(220), and 77.2(311) for metallic Ag (JCPDS No. 87-0720). SiO_2 nanoparticles existed in an amorphous phase in all composite nanofibers, regardless of chemical composition and heating temperature.

A previous study of the preparation of TiO_2 nanofibers found that the development of an anatase phase commenced at temperatures as low as 500 °C, and

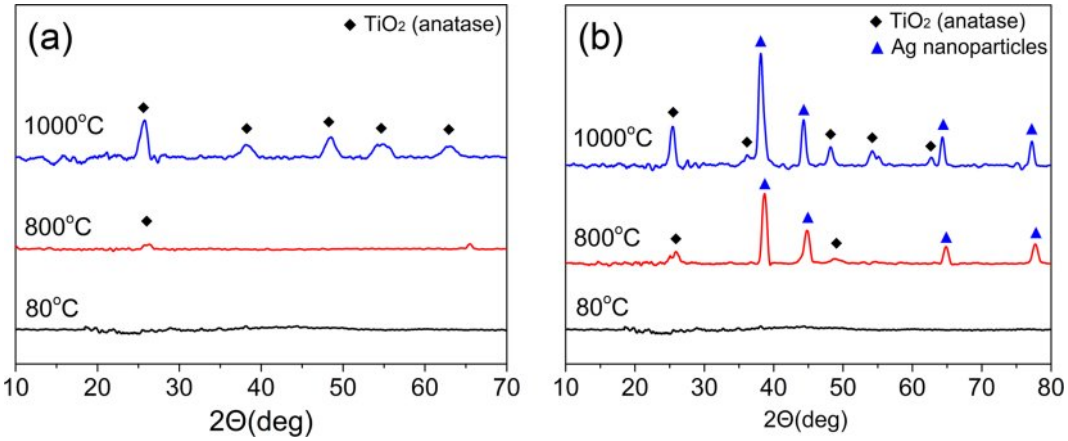

Fig. 4. XRD patterns of (a) TiO_2@SiO_2 and (b) TiO_2/Ag@SiO_2 composite nanofibers after drying (at 80 °C in a vacuum) and heat treatment at 800 °C and 1000 °C in air.

conversion of the anatase phase to the rutile phase was observed at temperatures as low as 600 °C. After 1000 °C heat treatment, only the rutile phase was observed [45]. The drying temperature of as-spun composite nanofiber did not have any effect on the morphology and crystallinity of inorganic composite nanofibers. On the other hand, the annealing temperature clearly affected the degree of crystallinity in inorganic composite nanofibers. For TiO_2@SiO_2 composite nanofibers, XRD analysis shows that the anatase phase appears after heat treatment at 800 °C. These relatively weak diffraction peaks increase further after heat treatment at 1000 °C while maintaining an anatase phase. It is possible that the homogeneous dispersion of TiO_2 nanoparticles in an amorphous SiO_2 matrix inhibits the phase transformation from anatase to rutile, preventing intimate crystal growth between TiO_2 nanoparticles [46]. For TiO_2/Ag@SiO_2 composite nanofibers, a similar trend in the development of an anatase phase in the XRD pattern is observed, although well-developed metallic Ag diffraction peaks appear even after heat treatment at 800 °C. Therefore, an annealing temperature of 1000 °C was selected as the annealing condition because a well-defined degree of crystallinity in an anatase phase was observed at this temperature.

A Debye-Scherrer analysis indicates that, after heating at 1000 °C, the average size of the crystalline anatase was 9.25 nm for TiO_2@SiO_2 composite nanofibers, and those of TiO_2 and metallic Ag were 10.38 nm and 10.34 nm, respectively, for TiO_2/Ag@SiO_2 inorganic composite nanofibers.

Fig. 5 and 6 show typical XPS survey spectra and high-resolution spectra for the Si2p, Ti2p, and Ag 3d regions of inorganic composite nanofibers before and after surface etching. TiO_2@SiO_2 inorganic composite nanofibers consist of the Si, O, and Ti elements, and the binding energies of Si2p, O1s, $Ti2p^1$, and $Ti2p^3$ are 102.6, 531, 464.5, and 458.4 eV, respectively. In the TiO_2/Ag@SiO_2 inorganic composite nanofibers, Ag was

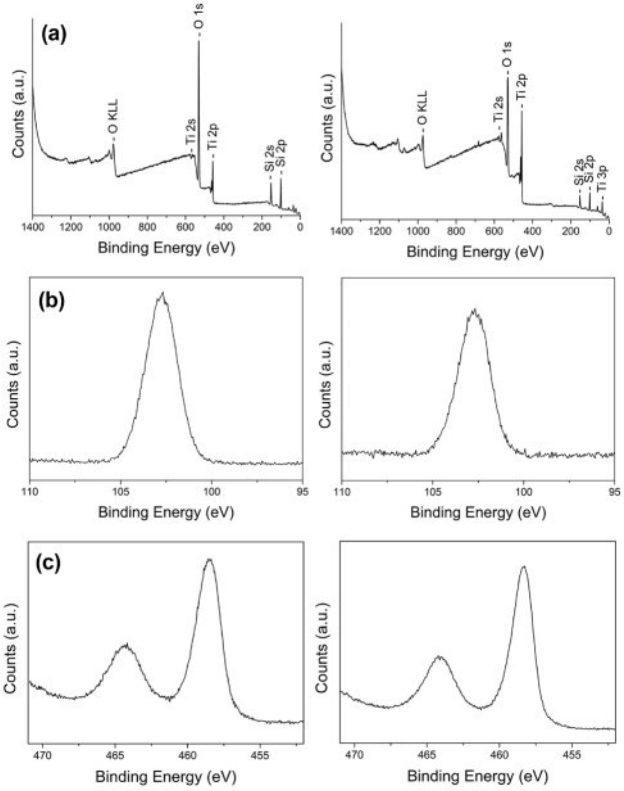

Fig. 5. XPS spectra of TiO_2@SiO_2 inorganic composite nanofibers before (left) and after (right) surface etching: (a) survey spectra and high-resolution images of (b) Si2p and (c) Ti2p.

found in addition to the other three elements. The binding energies of $Ag3d^3$ and $Ag3d^5$ bands for metallic Ag are 374.3 and 368.3 eV. The binding energy difference of the Ag3d was 6.0 eV, confirming the metallic chemical state of Ag, which agrees with previous reports [33, 47].

The UV-visible light spectra of the rhodamine B solution in the presence of inorganic composite nanofibers under UV irradiation were obtained to measure

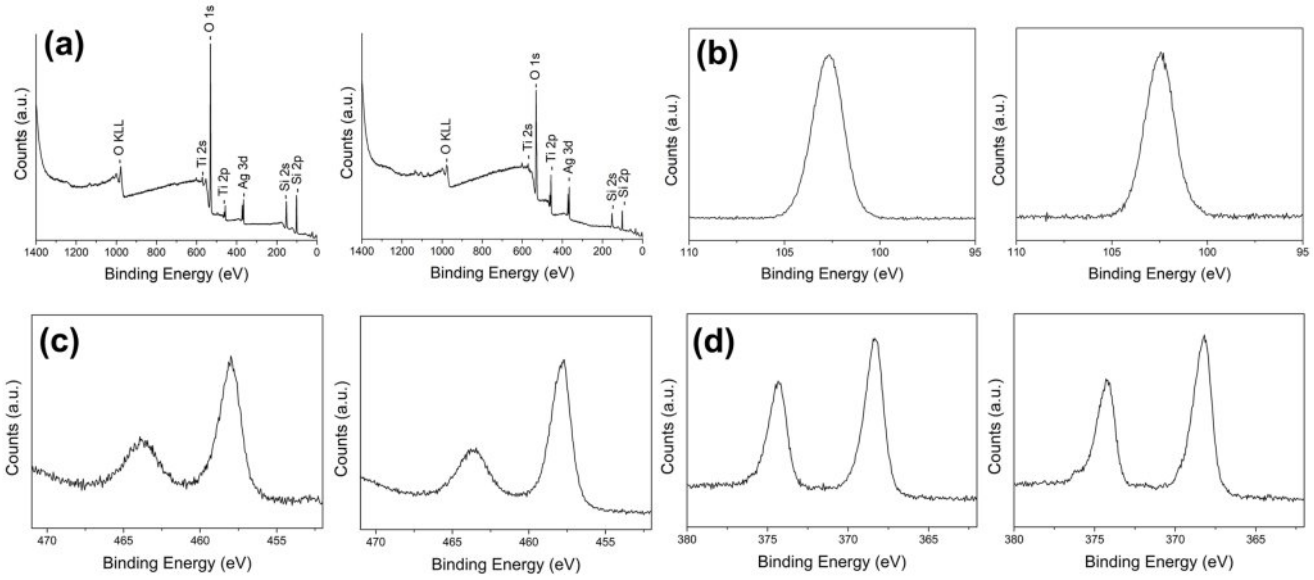

Fig. 6. XPS spectra of TiO_2/Ag@SiO_2 inorganic composite nanofibers before (left) and after (right) surface etching: (a) survey spectra and high-resolution images of (b) Si2p, (c) Ti2p, and (c) the Ag3d region.

photocatalytic degradation efficiencies (Fig. 7). The change in absorbance of the peak at 554 nm, the highest in the spectrum, was used to calculate the degradation percentages. The intensities of the absorbance peaks of rhodamine B decreased with an increase in irradiation time in the presence of photocatalysts. In all cases, a pretreatment time of 30 min in the dark before irradiation was used to ensure an adsorption and desorption equilibrium. As in Fig. 7(a), the absorbance peak at 554 nm in the photolysis sample containing TiO_2@SiO_2 inorganic composite nanofibers before surface etching decreased as follows: absorbance values of 0.80, 0.66,

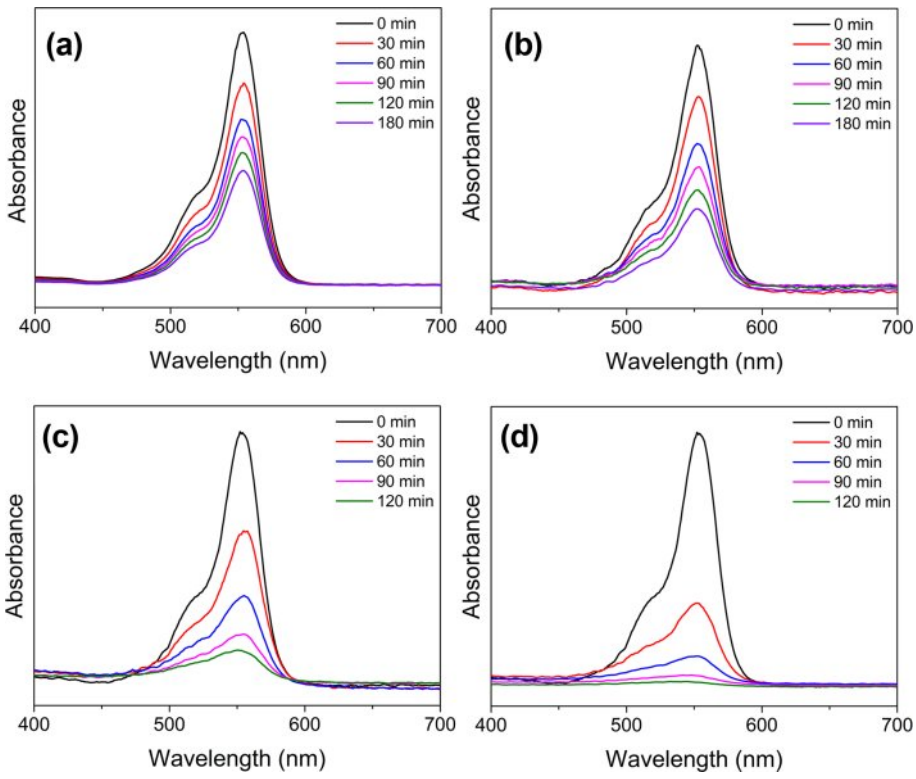

Fig. 7. UV-vis spectroscopic analysis of photocatalytic degradation of rhodamine B by TiO_2@SiO_2 (left) and TiO_2/Ag@SiO_2 (right) inorganic composite nanofibers (a), (b) before and (c), (d) after surface etching.

0.59, 0.42, and 0.45 after an irradiation time of 30, 60, 90, 120, and 180 min, respectively. For the photolysis sample containing TiO_2@SiO_2 inorganic composite nanofibers after surface etching, the absorbances were 0.61, 0.36, 0.21, and 0.15 for irradiation times of 30, 60, 90, and 120 min, respectively, as shown in Fig. 7(b). TiO_2/Ag@SiO_2 inorganic composite nanofibers before surface etching are presented in Fig. 7(c); the decrease in absorbance was from 0.77 to 0.60, 0.46, 0.40, and 0.33 after 30, 60, 90, 120, and 180 min of the irradiation time, respectively. Fig. 7(d) shows a decrease in absorbance for TiO_2/Ag@SiO_2 inorganic composite nanofibers after surface etching, exhibiting the most pronounced decrease in absorbance among all photocatalysts studied: absorbances of 0.33, 0.13, 0.05, and 0.03 for irradiation times of 30, 60, 90, and 120 min, respectively.

The photocatalytic performance of inorganic composite nanofibers was investigated by calculating the percentage of rhodamine B degradation as it varied with photocatalysis time under UV light. The amount of degradation of each inorganic composite nanofiber was obtained by measuring the value of C/C_0, where C and C_0 are the remainder and initial concentrations of rhodamine B, respectively. A comparative analysis revealed that the decrease in C/C_0 of rhodamine B with TiO_2/Ag@SiO_2 inorganic composite nanofibers was higher than that of TiO_2@SiO_2 inorganic composite nanofibers [48]. The percentages of degradation for TiO_2@SiO_2 inorganic composite nanofibers before surface etching at irradiation times of 30, 60, 120, and 180 min were 20.0%, 34.5%, 476.6%, and 54.6%, respectively, showing the lowest efficiency of degradation for rhodamine B among inorganic composite nanofibers employed. In the TiO_2/Ag@SiO_2 inorganic composite nanofibers before surface etching, the degradation ratios were 23.1%, 40.4%, 60.5%, and 67.2% after irradiation for 30, 60, 120, and 180 min, respectively, with slightly enhanced degradation efficiency upon addition of Ag. The proportions of degradation for TiO_2@SiO_2 inorganic composite nanofibers after surface etching were 38.8%, 64.1%, 85.4%, and 90.8% after irradiation for 30, 60, 120, and 180 min, respectively, yielding superior degradation efficiency compared with that of TiO_2@SiO_2 inorganic composite nanofibers before surface etching. The highest percentage of degradation was observed for TiO_2/Ag@SiO_2 inorganic composite nanofibers after surface etching, with degradation proportions of 66.8%, 87.5%, 97.4%, and 99.5% after irradiation for 30, 60, 120, and 180 min, respectively. For TiO_2/Ag@SiO_2 inorganic composite nanofibers after surface etching, less than an hour of irradiation was necessary to decompose 90% of organic dye, and rhodamine B was almost completely decomposed after 3 h of irradiation. We can conclude that, to construct the high-efficiency photocatalyst, the existence of photocatalytically active species such as TiO_2 on the surface of composite nanofiber catalysts is important, along with contributions from a noble metal

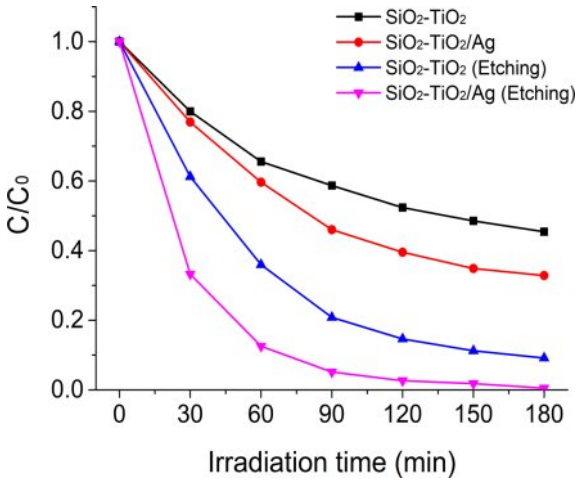

Fig. 8. Photocatalytic degradation of rhodamine B with UV irradiation for inorganic composite nanofibers before and after surface etching.

such as Ag [48, 49].

In wider and practical applications, the stability (or recyclability) of photocatalysts is an important factor. To investigate the photo-stability of inorganic composite nanofibers, the photocatalysts underwent three continuous cycles of photocatalysis of rhodamine B under identical conditions. In other previous studies on the recyclability of TiO_2/Ag@SiO_2 photocatalyst, it was reported that the photocatalytic efficiency remained practically constant, maintaining higher than 90% in each cycle with a total loss of less than 6% even after 5 to 10 cycles [50, 51]. However, an investigation of the effect of Ag dopant on recyclability has not been done in any of these studies, and no clear explanation was presented. In this study, analogous phenomena on the recyclability were observed for inorganic composite nanofibers, as shown in Fig. 9. For TiO_2/Ag@SiO_2 inorganic composite nanofibers after surface etching, the photocatalytic efficiency was maintained over 94% with the total loss of only 3.3% after 3 cycles. Compared TiO_2/Ag@SiO_2 inorganic composite nanofibers after surface etching, un-doped inorganic composite nanofibers after surface etching and both doped and un-doped inorganic composite nanofibers before surface etching exhibited low photocatalytic efficiencies along with huge total losses after 3 cycles. For TiO_2@SiO_2 inorganic composite nanofibers before surface etching, the photocatalytic efficiency decreased from 54.6% to 47.0%, with a loss of 7.6% after 2 cycles. For TiO_2@SiO_2 inorganic composite nanofibers after surface etching, the photocatalytic efficiency decreased from 67.2% to 61.6% and 57.3%, with a loss of 5.6% and 4.3% after the second and third cycles. Surface etching of inorganic composite nanofibers augmented the photocatalytic ability by increasing the surface area and exposing additional photocatalytic active sites, such as TiO_2 and metallic Ag nanoparticles. About 10~15% improvement in the photocatalytic efficiency was

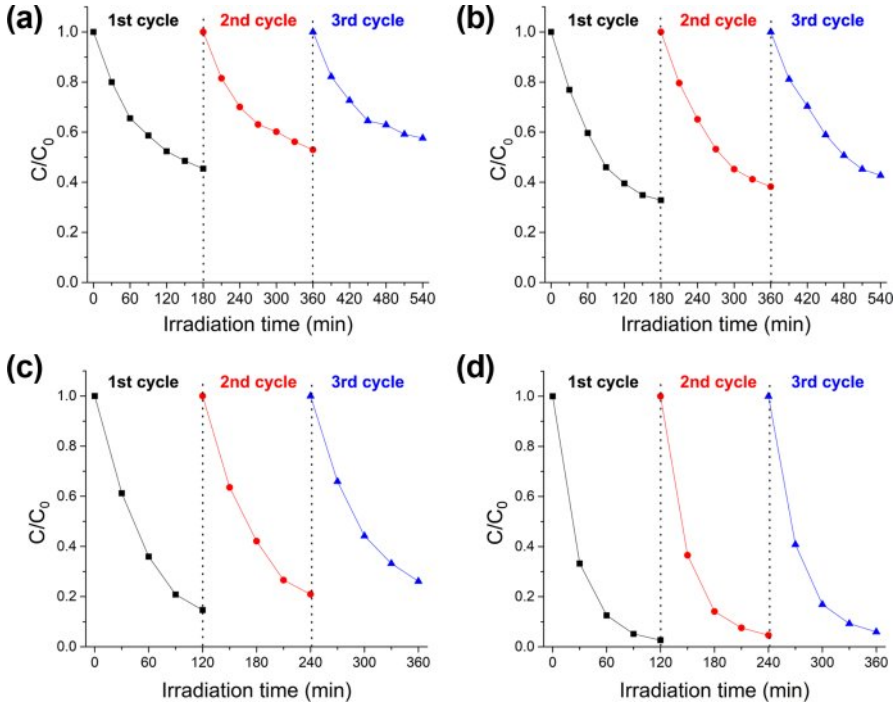

Fig. 9. Recycling properties of photocatalytic degradation of rhodamine B by TiO_2@SiO_2 inorganic composite nanofibers (left) before (a) and after (b) surface etching and TiO_2/Ag@SiO_2 inorganic composite nanofibers (right) before (c) and after (d) surface etching.

achieved by surface etching with HF, while the difference in the loss was 2% after 2 cycles. For TiO_2/Ag@SiO_2 inorganic composite nanofibers before surface etching, the photocatalytic efficiency decreased from 85.4% to 79.1% and 73.9%, with a loss of 6.3% and 5.2% after second and third cycles. In the case of TiO_2/Ag@SiO_2 inorganic composite nanofibers, 12~20% enhancement in the photocatalytic efficiency was attained by surface etching with HF, and the difference in the loss was 4.3% and 3.9% after the second and third cycles. As described earlier, the incorporation of Ag nanoparticles into TiO_2@SiO_2 photocatalyst provides the formation of the Schottky barrier at the interfaces with TiO_2 that act as an electron-trapping center for the photo-generated electrons, thereby preventing the electron-holes pairs recombination. Therefore, compared to un-doped photocatalyst, Ag doped TiO_2@SiO_2 photocatalyst can supply more electrons and holes to participate in the reaction with water, oxygen, and organic matter and exhibit more enhanced photocatalytic efficiency as well as recyclability.

Conclusions

Inorganic composite nanofibers with enhanced photocatalytic activity were fabricated using an electrospinning technique followed by thermal treatment. Two composite hybrid nanofibers (TiO_2@SiO_2 and TiO_2/Ag@SiO_2) were prepared by mixing corresponding chemical species such as $Ti(acac)_2(O^iPr)_2$, Ag-ND, and PTMS-based ORMOSIL particles in DMF. Subsequent heat treatment at 1000 °C converted these as-spun hybrid composite nanofibers to inorganic composite nanofibers. Under UV light, TiO_2/Ag@SiO_2 inorganic composite nanofibers showed significantly enhanced photocatalytic activity compared with TiO_2@SiO_2 inorganic composite nanofibers. The enhanced photocatalytic performance of TiO_2/Ag@SiO_2 inorganic composite nanofibers is likely due to the successful utilization of metallic Ag nanoparticles in composite nanofibers by providing efficient charge separation through the overlapping of band structures of Ag and TiO_2. Surface etching of inorganic composite nanofibers with an aqueous solution of HF can further increase photocatalytic activity by exposing more photocatalytically active TiO_2 and metallic Ag nanoparticles on the surface of inorganic composite nanofibers. Both inorganic composite nanofibers are recyclable, and their photocatalytic activities did not change noticeably over three repeated photodegradation tests under identical experimental conditions. Characterization using XRD, TEM-EDS, and XPS confirmed the uniform distribution of constituent nanoparticles (TiO_2 and metallic silver) and the structural integrity of composite nanofibers. These findings suggest that the inorganic composite nanofibers developed in this study possess excellent photocatalytic properties and the potential to be applied to diverse industrial applications.

Conflicts of interest

There are no conflicts to declare.

Author Contributions: Hyung Jun Lim and Gyu Il Jung equally contributed to this study as first authors by designing experiments, performing the experimental work, and writing the manuscript. Da Young Kang contributed to this manuscript by performing the experimental work and characterizing the materials.

Acknowledgments

This work was supported by the Technology Innovation Program (20023290, Development of monodisperse silica manufacturing technology with a coefficient of variation (CV) of 3% under using silicon alkoxide-based sol-gel process) funded by the Ministry of Trade, Industry, & Energy (MOTIE, Korea).

References

1. J. Zhang, Y. Cai, X. Hou, H. Zhou, H. Qiao, and Q. Wei, J. Phys. Chem. C 122 (2018) 8946-8953.
2. J. Pan, Z. Dong, B. Wang, Z. Jiang, C. Zhao, J. Wang, C. Song, Y. Zheng, and C. Li, Appl. Catal. B 242 (2019) 92-99.
3. X. Huang, Q. Guo, B. Yan, H. Liu, K. Chen, S. Wei, Y. Wu, and L. Wang, J. Mol. Liq. 322 (2021) 114965.
4. S.J. Bu, Z.G. Jin, X.X. Liu, L.R. Yang, and Z.J. Cheng, J. Eur. Ceram. Soc. 25 (2005) 673-679.
5. M. Wark, J. Tschirch, O. Bartels, D. Bahnemann, and J. Rathouský, Microporous Mesoporous Mater. 84 (2005) 247-253.
6. Z. Ma, S. Brown, S.H. Overbury, and S. Dai, Appl. Catal. A 327 (2007) 226-237.
7. J. Yang, J. Zhang, L. Zhu, S. Chen, Y. Zhang, Y. Tang, Y. Zhu, and Y. Li, J. Hazard. Mater. 137 (2006) 952-958.
8. R. Hatefi, H. Younesi, A. Mashinchian-Moradi, and S. Nojavan, Adv. Powder Technol. 32 (2021) 2410-2422.
9. Y. Kang, K. Song, J. Park, Y.C. Kim, and S. Oh, J. Ceram. Process. Res. 14 (2013) 419-425.
10. Q. Du, J. Wu, and H. Yang, ACS Catal. 4 (2013) 144-151.
11. C. Song, S.K. Koppala, and J. Yoon, J. Ceram. Process. Res. 14 (2013) 653-657.
12. K.-Y.A. Lin, T.-Y. Lin, Y.-C. Lu, J.-T. Lin, and Y.-F. Lin, Chem. Eng. Sci. 168 (2017) 372-379.
13. S. Akhavan-Mahdavi, M.S. Mirbagheri, E. Assadpour, M.A. Sani, F. Zhang, and S.M. Jafari, Adv. Colloid Interface Sci. 325 (2024) 103111.
14. Q. Zhang, J. Welch, H. Park, C.-Y. Wu, W. Sigmund, and J.C.M. Marijnissen, J. Aerosol Sci. 41 (2010) 230-236.
15. X. Li, W. Chen, Q. Qian, H. Huang, Y. Chen, Z. Wang, Q. Chen, J. Yang, J. Li, and Y.-W. Mai, Adv. Eng. Mater. 11 (2020) 2000845.
16. A.Z. Sadek, J.G. Partridge, D.G. McCulloch, Y.X. Li, X.F. Yu, W. Wlodarski, and K. Kalantar-zadeh, Thin Solid Films 518 (2009) 1294-1298.
17. V. Ganapathy, B. Karunagaran, and S.-W. Rhee, J. Power Sources, 195 (2010) 5138-5143.
18. Y. Lara-López, G. García-Rosales, and J. Jiménez-Becerril, J. Ceram. Process. Res. 20 (2019) 24-29.
19. A.R. Malagutti, H.A.J.L. Mourão, J.R. Garbin, and C. Ribeiro, Appl. Catal. B 90 (2009) 205-212.
20. P. Qu, J. Zhao, T. Shen, and H. Hidaka, J. Mol. Catal. A Chem. 129 (1998) 257-268.
21. R. Libanori, T.R. Giraldi, E. Longo, E.R. Leite, and C. Ribeiro, J. Sol-Gel Sci. Technol. 49 (2009) 95-100.
22. D. Li, and Y. Xia, Nano Lett. 3 (2003) 555-560.
23. T. He, Z. Zhou, W. Xu, F. Ren, H. Ma, and J. Wang, Polymer 50 (2009) 3031-3036.
24. S.U.M. Khan, M. Al-Shahry, and W.B. Ingler Jr, Science 297 (2002) 2243-2245.
25. M. Pelaez, N.T. Nolan, S.C. Pillai, M.K. Seery, P. Falaras, A.G. Kontos, P.S.M. Dunlop, J.W.J. Hamilton, J.A. Byrne, K. O'Shea, M.H. Entezari, and D.D. Dionysiou, Appl. Catal. B 125 (2012) 331–349.
26. J.-M. Herrmann, H. Tahiri, Y. Ait-Ichou, G. Lassaletta, A.R. González-Elipe, and A. Fernández, Appl. Catal. B 13 (1997) 219-228.
27. B. Li, Y. Hao, X. Shao, H. Tang, T. Wang, J. Zhu, and S. Yan, J. Catal. 329 (2015) 368-378.
28. S. Ryu, J.W. Chung, and S. Kwak, Compos. Sci. Technol. 117 (2015) 9-17.
29. J. Ma, Z. Xiong, T.D. Waite, W.J. Ng, and X.S. Zhao, Microporous Mesoporous Mater. 144 (2011) 97-104.
30. E.D. Jeong, P.H. Borse, J.S. Jang, J.S. Lee, O. Jung, H. Chang, J.S. Jin, M.S. Won, and H.G. Kim, J. Ceram. Process. Res. 9 (2008) 250-253.
31. Y. Song, M. Lee, B. Kim, and D.Y. Lee, J. Ceram. Process. Res. 20 (2019) 182-186.
32. Y. Song, Y. Peng, N.V. Long, Z. Huang, and Y. Yang, Appl. Surf. Sci. 542 (2021) 148584.
33. M. Tahir, J. CO2 Util. 37 (2020) 134-146.
34. J. Shen, Y. Zhou, J. Huang, Y. Zhu, J. Zhu, X. Yang, W. Chen, Y. Yao, S. Qian, H. Jiang, and C. Li, Appl. Catal. B 205 (2017) 11-18.
35. Y. Zhang, T. Wang, M. Zhou, Y. Wang, and Z. Zhang, Ceram. Int. 43 (2017) 3118-3126.
36. L. Zhang, C. Ni, H. Jiu, C. Xie, J. Yan, and G. Qi, Ceram. Int. 43 (2017) 5450-5456.
37. C.Y. Jung, J.S. Kim, H.Y. Kim, J.M. Ha, Y.H. Kim, and S.M. Koo, J. Colloid Interface Sci. 367 (2012) 67-73.
38. A. Jitianu, G. Amatucci, and L.C. Klein, J. Am. Ceram. Soc. 92 (2009) 36-40.
39. J.S. Kim, G.I. Jung, S.J. Kim, and S.M. Koo, J. Nanopart. Res. 20 (2018) 73.
40. D.D. Evanoff Jr, and G. Chumanov, Chemphyschem 6 (2005) 1221-1231.
41. X. Li, S. Raza, and C. Liu, J. Environ. Chem. Eng. 9 (2021) 106133.
42. Z. Duan, Y. Huang, D. Zhang, and S. Chen, Sci. Rep. 9 (2019) 8008.
43. X. Long, D. Yu, J. Han, Z. Huang, J. Xiao, G. Feng, J. Zhu, and K. Yang, Opt. Express 32 (2024) 21304-21326.
44. D. Nagy, C. Chao, B. Marzec, F. Nudelman, M.-C. Ferrari, and X. Fan, J. Environ. Manage. 260 (2020) 110175.
45. P. Viswanathamurthi, N. Bhattarai, C.K. Kim, H.Y. Kim, and D.R. Lee, Inorg. Chem. Commun. 7 (2004) 679-682.
46. S.F. Resende, E.H.M. Nunes, M. Houmard, and W.L. Vasconcelos, J. Colloid Interface Sci. 433 (2014) 211-217.
47. Z. Wang, A.A. Haidry, L. Xie, A. Zavabeti, Z. Li, W. Yin, R.L. Fomekong, and B. Saruhan, Appl. Surf. Sci. 533 (2020) 147383.
48. A. Al Baroot, S.A. Haladu, S.M. Magami, S. Akhtar, Q.A. Drmosh, K.A. Elsayed, and A.A. Manda, J. Phys. Chem. Solids 180 (2023) 111489.
49. H.-R. Xu, P.-Y. Lee, Y.-W. Tsai, and Y.-C. Lee, J. Ceram. Process. Res. 22 (2021) 179-185.
50. L. Aoudjit, H. Salazar, D. Zioui, A. Sebti, P.M. Martins, and S. Lanceros-Mendez, Polymers 13 (2021) 3718.
51. E.M. Abdelsalam, Y.M.A. Mohamed, S. Abdelkhalik, H.A. El Nazer, and Y.A. Attia, Environ. Sci. Pollut. Res. 27 (2020) 35828-35836.